energies

MDPI

Article

Structure and Thermophysical Properties of Molten Calcium-Containing Multi-Component Chlorides by Using Specific BMH Potential Parameters

Xiaolan Wei [1], Dandan Chen [1], Shule Liu [2,*], Weilong Wang [2,*], Jing Ding [2] and Jianfeng Lu [2]

[1] School of Chemistry and Chemical Engineering, South China University of Technology, Guangzhou 510640, China
[2] School of Materials Science and Engineering, Sun Yat-Sen University, Guangzhou 510006, China
* Correspondence: liushle@mail.sysu.edu.cn (S.L.); wwlong@mail.sysu.edu.cn (W.W.)

Abstract: Chloride molten salts have become a potential heat storage material for the design of a new generation of concentrating solar power (CSP) (>700 °C) due to its abundant reserves and low cost. The difficulty of measuring the high-temperature thermal properties of chlorides can be effectively solved by using molecular dynamics simulation. However, it is challenging to get the thermophysical properties of multi-component molten salts containing $CaCl_2$ due to the lack of Born–Mayer–Huggins (BMH) potential parameters of $CaCl_2$. Through comparative analysis of the structure and thermal properties of $CaCl_2$, including density and thermal conductivity, a set of Born–Mayer–Huggins (BMH) potential parameters of $CaCl_2$ named SP2 is determined in this study. The density, specific heat capacity, and thermal conductivity of nine eutectic molten salts are simulated, including NaCl-$CaCl_2$, KCl-$CaCl_2$, NaCl-$CaCl_2$-$MgCl_2$, and NaCl-$CaCl_2$-KCl, and the simulation results are found to be in good agreement with the experimental results. It is also found that the SP2 parameters are able to predict the thermal properties and structure of molten multicomponent chlorides including calcium.

Keywords: calcium chloride; classical molecular dynamics simulation; BMH potential parameters; thermophysical properties; structure

Citation: Wei, X.; Chen, D.; Liu, S.; Wang, W.; Ding, J.; Lu, J. Structure and Thermophysical Properties of Molten Calcium-Containing Multi-Component Chlorides by Using Specific BMH Potential Parameters. *Energies* **2022**, *15*, 8878. https://doi.org/10.3390/en15238878

Academic Editor: Lyes Bennamoun

Received: 13 October 2022
Accepted: 21 November 2022
Published: 24 November 2022

1. Introduction

Due to the high heat storage density and good fluidity at high temperatures, molten salts can be used as fuel coolant in nuclear reactors and heat storage material in concentrating solar power (CSP). Nitrate and nitrite are commonly used heat storage materials for CSP [1,2], but their maximum operating temperature is only 565 °C [3]. To improve the energy conversion efficiency, it is necessary to develop a new kind of heat transfer fluid and heat storage media for the next generation of CSP (>700 °C). Chloride molten salt is a potential heat storage material for a new generation of CSP with the feature of abundant reserves, low cost, and high upper operating temperatures. Especially, calcium chloride ($CaCl_2$) molten salt has a high melting point and good stability, which can be used to design and develop chloride eutectic molten salts as heat storage materials. Wei et al. [4] studied the specific heat capacity c_p, density ρ, viscosity η, and thermal stability of six chloride molten salt materials, including NaCl-$CaCl_2$, NaCl-KCl-$CaCl_2$, NaCl-$CaCl_2$-$MgCl_2$, KCl-$CaCl_2$-$MgCl_2$, NaCl-KCl-$MgCl_2$, and NaCl-KCl-$CaCl_2$-$MgCl_2$. The comparison shows that NaCl-KCl-$CaCl_2$ has a good energy storage density and can operate stably at 520–900 °C. Tian et al. [5] compared the thermophysical properties and economic benefits of binary chloride eutectic molten salt (NaCl-$CaCl_2$ 52–48 mol %) with commercial nitrate, and the results showed that this chloride eutectic molten salt was a promising high-temperature heat storage material. It is difficult to measure molten calcium-containing multi-component chlorides by using existing test methods due to their high-temperature condition and corrosions. So far, quite a few experimental values of thermal properties at high temperatures have been obtained, but they remain limited to a small temperature range above the melting

point. To develop the application of a calcium-containing multi-component chloride molten salt in the field of heat transfer and energy storage, complete thermophysical property data for the whole working temperature range are required.

Both classical molecular dynamics simulation and first-principles molecular dynamics (FPMD) simulation are effective ways to predict the macroscopic thermal properties of materials. Compared to FPMD, the classical molecular dynamic simulation can calculate a larger system, which requires less calculation. Especially regarding the molten salts in the existent of ions, the heat transfer and storage properties at high temperature can be predicted to analyze its microstructure mechanism by classical molecular dynamics simulation. Pan et al. [6] simulated the thermophysical properties and transport properties of monovalent alkali metal chloride molten salt by classical molecular dynamics simulation. The Born–Mayer–Huggins potential was used to describe the interaction between chloride ions and the thermal conductivity and viscosity of molten chlorides were calculated by reverse non-equilibrium molecular dynamics (RNEMD) method. The simulation results show that RNEMD can accurately simulate the transport properties of monovalent alkali metal chloride molten salt. Xie et al. [7] calculated the thermal properties of the microstructure of binary eutectic salt LiCl-KCl by classical molecular dynamics simulation, and the error between the simulation value and the experimental value is within 11.1%. It can be seen that the classical molecular dynamics simulation method is available for predicting the thermophysical properties of monovalent alkali metal chloride molten salt at high temperatures. However, the classical molecular dynamics simulation potential parameters of alkaline earth metal chloride molten salts are very scarce, especially those containing $CaCl_2$.The simulation of eutectic molten salt of molten calcium-containing multicomponent chlorides is based on the first-principles calculation. Bu et al. [8] calculated the structure of high-temperature $CaCl_2$ by FPMD but did not calculate other thermal properties limited by small calculation amount and system size. Rong et al. [9,10] analyzed the microstructure of NaCl-$CaCl_2$ and NaCl-$CaCl_2$-$MgCl_2$ by FPMD and calculated the related thermophysical properties. Igarashi et al. [11,12] analyzed the structure of $CaCl_2$-KCl by classical molecular dynamics compared with the results of XRD and Raman scattering. It was found that $CaCl_2$ in this system mainly existed as an octahedral structure. However, the simplified potential function is used in the literature, which only consists of the Coulombic and the repulsive term, and the research only stays in the analysis of microstructure, without further analysis and prediction of thermal properties at high temperature. In this paper, a more detailed potential function is used to describe the interaction between $CaCl_2$ particles, and the structure and properties of molten calcium-containing multi-component chlorides are further studied.

In this work, by simulating the structure and thermal properties of molten $CaCl_2$, a set of potential parameters suitable for molecular dynamics simulations of molten $CaCl_2$ and molten calcium-containing multi-component chlorides were established based on the studies of divalent metal halides and $CaCl_2$ molten salts that have already been conducted. The structure of NaCl-$CaCl_2$, KCl-$CaCl_2$, NaCl-KCl-$CaCl_2$, and NaCl-$CaCl_2$-$MgCl_2$ were simulated by using the BMH potential parameters of $CaCl_2$ determined in this paper. Subsequently, the thermophysical properties of molten calcium-containing multi-component chlorides were also calculated, including density, specific heat capacity, and thermal conductivity.

2. Model and Methodology

2.1. Physical Model

The initial model of unit $CaCl_2$ extends a $5 \times 5 \times 24$ supercell in X, Y, and Z directions, which consists of 3600 particles. The simulation systems of multi-component eutectic salts NaCl-$CaCl_2$, KCl-$CaCl_2$, NaCl-KCl-$CaCl_2$, and NaCl-$CaCl_2$-$MgCl_2$ are set to 4000 molecules. The number of particles of each component is determined by a molar fraction, and the initial density of the system determines the size of the square simulation box. PACKMOL [13] was used to construct the initial model of multi-element eutectic molten salt.

2.2. Force Field

The selection of force field and the determination of potential parameters are the key for molecular dynamics simulations. The Fumi-Tosi potential is usually used in chloride [2,14,15] molten salts. For the simulation of the structure and thermophysical properties of chloride molten salts, the intermolecular potential function adopts the Born–Mayer–Huggins (BMH) potential energy model:

$$U_{ij}^{Fumi-Tosi} = \frac{q_i q_j e^2}{r_{ij}} + A_{ij}\exp\left(\frac{\sigma_{ij} - r_{ij}}{\rho_{ij}}\right) - \frac{C_{ij}}{r_{ij}^6} - \frac{D_{ij}}{r_{ij}^8} \quad (1)$$

$$A_{ij} = b(1 + \frac{q_i}{n_i} + \frac{q_j}{n_j}) \quad (2)$$

$$\sigma_{ij} = \sigma_i + \sigma_j \quad (3)$$

In Equation (1), the four terms on the right-hand side represent the long-range Coulomb electrostatic force (first term), the short-range repulsive force due to overlapping electron clouds (second term) and the van der Waals attraction due to ion polarization (third and fourth terms), respectively. A_{ij} in the second term can be calculated using Equation (2), where b represents the strength of the repulsive force ($b = 1.90 \times 10^{-20}$ J/molecule) [16]; n_i is the outermost electron of the ion i; where e is the unit electronic charge, q_i and q_j are the charge numbers of the ions (where qNa/K = 1, qCa/Mg = 2, qCl = −1). r_{ij} is the distance between i and j ions. σ_i and σ_j are the radii of i and j ions, and ρ_{ij} is the hardening parameter between i and j ions. C_{ij} and D_{ij} are the dipole–dipole interaction coefficients and dipole-quadrupole interaction coefficients.

Woodcoc [16] et al. have studied zinc chloride using molecular dynamics simulations, and it was found that the dipolarization forces of zinc chloride can cancel each other out. Calcium chloride is a divalent metal halide similar to zinc chloride. Therefore, in this study, both C_{ij} and D_{ij} in the one-component calcium chloride potential parameter were set to zero. In the multicomponent chloride system dipolarization cannot be neglected, but the calcium ion has a large charge and small radius, so its dipolarization potential can be neglected, and only the dipolarization force of the anion pair in calcium chloride is considered. $C_{\text{Cl-Cl}}$ of $CaCl_2$ is 1845.45 kcal·Å^6/(mol) [17].

Based on the available literature, Table 1 listed three sets of BMH potential parameters for $CaCl_2$. To better predict the thermophysical properties of multi-component eutectic molten salt containing $CaCl_2$ and analyze its microscopic mechanism by molecular dynamics simulation, this study simulated and verified the accuracy of three sets of potential parameters of $CaCl_2$ in the Table 1. The BMH potential parameters of sodium chloride and potassium chloride used in this paper are already mature and can be directly cited from the [18], and the BMH potential parameters of $MgCl_2$ are taken from the work by Lu [19]. The interaction parameters of Cl^--Cl^- in polychlorinated molten salt are weighted average based on the mole fractions of each cation, and interaction parameters between different cations using mixing rules [20]: $(A_{12})^2 = A_{11}A_{22}$, $(C_{12})^2 = C_{11}C_{22}$, $(D_{12})^2 = D_{11}D_{22}$, $2/\rho_{12} = 1/\rho_{11} + 1/\rho_{22}$.

Table 1. Born-Mayer-Huggins potential parameters of $CaCl_2$ [6,11,16,17,21].

Parameters	A_{ij} (kcal/mol)			σ_{ij} (Å)			ρ_{ij} (Å)		
	Ca-Ca	**Ca-Cl**	**Cl-Cl**	**Ca-Ca**	**Ca-Cl**	**Cl-Cl**	**Ca-Ca**	**Ca-Cl**	**Cl-Cl**
SP1 [11]	0.1597	0.1749	0.1889	2.814	3.357	3.900	0.160	0.170	0.190
SP2 [17,21]	4.0995	3.0746	2.0489	2.880 [11]	3.118	3.356 [16]	0.324 [17]	0.324	0.324
SP3 [6,16,17]	4.0995	3.0746	2.0489	2.180 [17]	2.675	3.170 [6]	0.324 [17]	0.324	0.324

2.3. Simulation Detail

The software used for the simulations was LAMMPS coded [22], and periodic boundary conditions (PBC) was chosen to create an infinite system. In order to eliminate the effect of mirror particle action on the long-range force calculation, the cutoff radius is set to 20 Å, which is slightly less than half of the simulated box edge length. The PPPM (particle-particle, particle-mesh) algorithm (with an accuracy of 1.0×10^{-6}) is used to reduce the truncation error and perform the long-range correction. The initial velocity is given according to the potential parameters and obeys a Gaussian distribution. The Newtonian equation of motion is solved by the Verlet [23] computing method. For all simulated systems, the simulated annealing equilibrium was performed using the NPT ensemble with a Nosé–Hoover thermostat and a constant pressure of 0.1 MP. Firstly, it was heated to the upper temperature of the simulated temperature range and then cooled to a different simulated temperature. At the equilibrium volume, the system is analyzed and calculated using the NVT ensemble with the simulation time step set to 1 fs. The equilibration time for each simulation is 1 ns in order to obtain accurate calculation results.

2.4. Experimental

2.4.1. Materials

The analytically pure NaCl, $CaCl_2$, and anhydrous $MgCl_2$ (AR, ≥99% purity, Guangzhou Chemical Co., Ltd., Guangzhou, China) after drying for 24 h were mechanically mixed. Then, they were put into a muffle furnace and heated for 3 h at 600 °C, and then cooled to room temperature. The prepared samples were vacuum sealed and preserved in anticipation of the tests of thermal properties.

2.4.2. Specific Heat Capacity Measurements

The differential scanning calorimeter (DSC 404F1 NETZSCH, uncertainty: ~±3%) was used to measure the specific heat capacity of the sample. The platinum crucible was selected as the measurement crucible. Under a nitrogen (N_2) atmosphere of 40 mL min^{-1}, a blank crucible was measured as the baseline. Then, the DSC curve of a sapphire was measured. Finally, the DSC curve of samples with similar sapphire quality was measured. The specific heat capacity of the sample was calculated by comparing Equation (4).

$$C_{p,\text{sample}} = \frac{DSC_{\text{sample}} - DSC_{\text{blank}}}{DSC_{\text{sapphire}} - DSC_{\text{blank}}} \frac{m_{\text{sapphire}}}{m_{\text{sample}}} C_{p,\text{sapphire}} \quad (4)$$

2.4.3. Density Measurements

The density is measured by the Archimedes method (uncertainty: ~±2%). The principle is that the buoyancy of platinum hammers in molten salts is equal to the weight of molten salt discharged. Therefore, the density of molten salt can be calculated according to Equation (5) according to the mass change of molten salt immersed by the platinum hammer. The measurement steps are as follows: Firstly, the weight of the platinum hammer in air and water is measured. Then, the platinum hammer is immersed in molten salt to record the weight of the platinum hammer at different temperatures. The density measurement temperature ranges of NaCl-$CaCl_2$ binary eutectic molten salt and NaCl-$CaCl_2$-$MgCl_2$ ternary eutectic molten salt are 550–650 °C and 470–600 °C, respectively. The test was conducted in the atmosphere of N_2.

$$\rho = \frac{m_{air} - m_{salt}}{\frac{m_{air} - m_{water}}{\rho_{water}}[1 + 3\alpha(T - 25)]} \quad (5)$$

where m is the weight of platinum hammer in different environments; α is the expansion coefficient of platinum hammer 0.000009, and T is the temperature of molten salt.

3. Properties Evaluation

3.1. Radial Distribution Function

The radial distribution function (RDF) is the spatial distribution of j particles in the range of radius r centered on i particles. It is an important function to describe the characteristics of fluid microstructure, which can be expressed as:

$$g_{ij}(r) = \frac{1}{4\pi\rho_j r^2}\left[\frac{\mathrm{d}N_{ij}(r)}{\mathrm{d}r}\right] \tag{6}$$

where $g_{ij}(r)$ is a radial distribution function, $N_{ij}(r)$ is the average number of j particles in the spherical shell away from i particles r~δ, and ρ_j is the number density of j particles.

3.2. Coordination Number

The coordination number is the average number of j particles in the first shell of $r_{\min}$, which is reflected in the distance from the i center particles. It is one of the most important parameters for the analysis of fluid microstructure and describes the tightness of particle arrangement in the system.

$$N_{ij}(r) = 4\pi\rho_j \int_0^{r_{\min}} g_{ij}(r) r^2 \mathrm{d}r \tag{7}$$

where $r_{\min}$ is the location of the valley of the first peak in the RDF.

3.3. Angular Distribution Function

The bond angle distribution function is calculated according to three particle coordinates, which reflect the order of the microstructure of the material. For the three particles *jik*, the bond angle centered on particle i can be expressed as:

$$\theta_{jik} = \left\langle \cos^{-1}\left(\frac{r_{ij}^2 + r_{ik}^2 - r_{jk}^2}{2r_{ij}r_{ik}}\right)\right\rangle \tag{8}$$

3.4. Density and Specific Heat Capacity

The density can be calculated by the volume after relaxation. After the system is balanced, the density will not change again.

$$\rho = \frac{m}{V} = \frac{NM}{N_\mathrm{a}V} \tag{9}$$

where ρ represents the density of the system, N is the number of simulated molecules, M is the molar mass of molecules, V is the equilibrium volume of the system, and N_a is the Avogadro constant.

Specific heat capacity is commonly used to represent the heat absorbed or released during the calculation of temperature change, which can be calculated by the following equation:

$$C_\mathrm{p} = \left(\frac{\partial H}{\partial T}\right) \approx \frac{\Delta H}{\Delta T} \tag{10}$$

where ΔT represents the temperature change of the systems and ΔH represents the change of enthalpy under the temperature change of ΔT.

3.5. Thermal Conductivity

In this paper, the reverse non-equilibrium molecular dynamics (RNEMD) simulation method [24] is adopted to calculate the thermal conductivity of chloride molten salt. RNEMD method simulates the kinetic energy exchange between the middle plate and the bottom plate of the box and measures the resulting temperature gradient [25]. The

kinetic energy exchange rate is 200 time steps, forming a linear temperature gradient. The calculation of thermal conductivity is as follows:

$$j_z = -\lambda \frac{\partial T}{\partial z} \tag{11}$$

$$\lambda = -\frac{\sum_{\text{transfer}} \frac{m}{2}\left(v_{\text{hot}}^2 - v_{\text{cold}}^2\right)}{2tL_xL_y(\partial T/\partial z)} \tag{12}$$

where λ is the thermal conductivity, $\left\langle \frac{\partial T}{\partial z} \right\rangle$ is the temperature gradient, L_x, L_y is the length of the simulation box in x, y direction, and t is the kinetic energy exchange time interval.

4. Result and Discussion

4.1. Structure and Density Verification of Molten Salt $CaCl_2$

4.1.1. Structure Calculation

Molecular dynamics simulation can analyze the relationship between the microstructure and macroscopic properties of molten salt. The simulation of high-temperature molten salt needs to be on the premise of reasonable structure, so as to accurately predict the physical properties of high-temperature sections that are difficult to achieve under experimental conditions. In this paper, the BMH potential parameters of three sets of $CaCl_2$ are sorted out, and the radial distribution and coordination number distribution of molten $CaCl_2$ at 1100 K are calculated, as shown in Figure 1. The coordination numbers $N_{\text{Ca-Cl}}$ of the first peak $R_{\text{Ca-Cl}}$ obtained from Figure 1 are listed in Table 2, and the related experimental measurement results of Biggin [26] and the calculated results using the first principle molecular dynamics (FPMD) simulations by Bu [8] are also listed in Table 2.

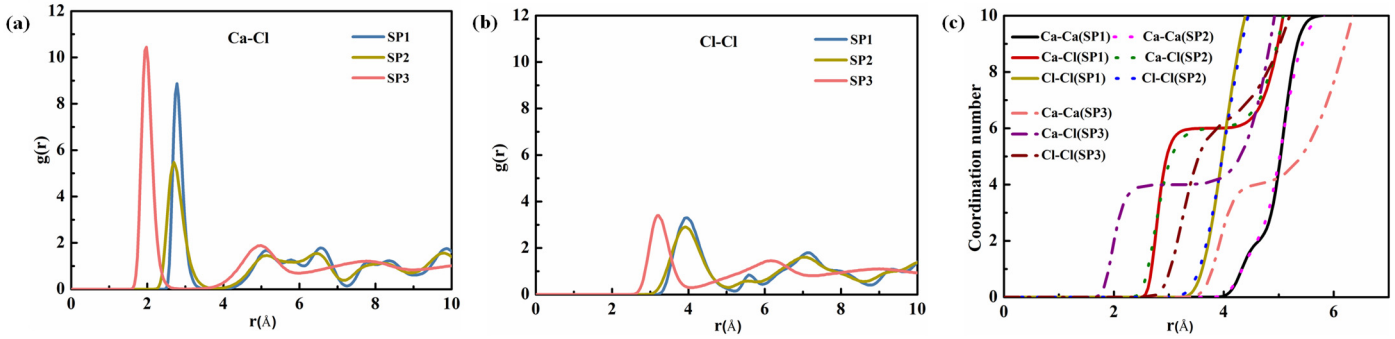

Figure 1. The radial distribution function of (**a**) Ca-Cl, (**b**) Cl-Cl; and (**c**) coordination number distribution in $CaCl_2$ calculated with different potential parameters.

Table 2. The first peak positions R of ions pairs of $CaCl_2$ and averaged coordination number N of molten $CaCl_2$ [8,26].

Method	T (K)	$R_{\text{Ca-Ca}}$ (Å)	$R_{\text{Ca-Cl}}$ (Å)	$R_{\text{Cl-Cl}}$ (Å)	$N_{\text{Ca-Cl}}$
SP1	1100 K	5.10	2.78	3.94	6
SP2	1100 K	4.98	2.70	3.94	6
SP3	1100 K	3.90	1.98	3.22	4
FPMD [8]	1100 K	4.52	2.71	3.64	6.3
Experiment [26]	1093 K	3.60	2.78	3.73	5.4

It can be seen from Table 2 that the first peak $R_{\text{Ca-Cl}}$ and $R_{\text{Cl-Cl}}$ of Ca-Cl and Cl-Cl ion pairs calculated by SP1 and SP2 have a good consistency. However, the first peak $R_{\text{Ca-Ca}}$ calculated by SP1 and SP2 was larger than the experimental value of Biggin [26]. The $R_{\text{Ca-Ca}}$ in $CaCl_2$ calculated by Min Bu [8] using the FPMD simulations is also significantly larger, which may be affected by the cation on the repulsion. The first peak $R_{\text{Ca-Cl}}$ of Ca-Cl ion

pair calculated by parameter SP3 was 1.98 Å, indicating that the atomic orbitals of Cl^- and Ca^{2+} overlap greatly, which contrary to the fact that $CaCl_2$ is a typical ionic compound. The ionic radii of Cl^- and Ca^{2+} are 1.81 Å and 0.99 Å [27], respectively, and the sum of their radii is 2.80 Å, which is close to the experimental value of 2.78 measured by Biggin [26]. Therefore, the $R_{Ca\text{-}Cl}$ value is more reasonable in the range of 2.70–2.78 showed in Table 2, i.e., Ca-Cl has orbital overlap but the degree is not large. Therefore, the calculation results of parameter SP3 are less reasonable.

As shown in Figure 1c, the coordination number distribution curves show that the coordination number of calcium in molten $CaCl_2$ calculated by parameter SP3 is 4, indicating that Ca and Cl atom keep the tetrahedral structure, which is also inconsistent with the actual measured six-coordinate structure of $CaCl_2$ showed in Table 2. The coordination number curves calculated by the parameters SP1 and SP2 are basically coincident, where the coordination number $N_{Ca\text{-}Cl}$ of Ca-Cl is 6.0, which is close to the coordination number $N_{Ca\text{-}Cl}$ = 5.4 obtained by Biggin [26] at 1093 K. Although the simulation results are slightly larger than the experimental results, it can be seen that $CaCl_2$ has six-coordinate octahedral structure in the liquid state. The simulation results of the radial distribution function and coordination number Ca-Cl show that the SP1 and SP2 potential parameter are more reasonable.

4.1.2. Thermophysical Properties Calculation

Density is the macroscopic reflection of molten salt microstructure. In this paper, three sets of parameters are analyzed from the perspective of physical properties by calculating the density change of $CaCl_2$ with temperature in the molten state. Figure 2a shows the comparison of densities calculated by three sets of parameters with experimental values. The results show that the error between the calculated values of SP1 and SP2 and the experimental values [28] is less than 3%, and the error of SP3 is 5%. It can be seen from the density simulation results that the parameters SP1 and SP2 are reasonable.

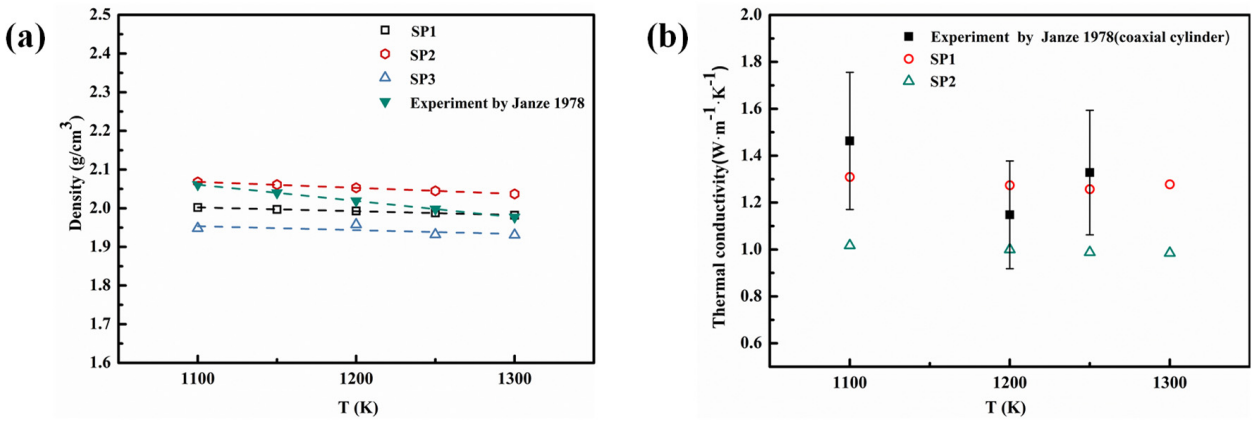

Figure 2. (**a**) Density of $CaCl_2$ varies with temperature; (**b**) Thermal conductivity of $CaCl_2$ changes with temperature [28].

Figure 2b illustrates the calculated thermal conductivity of $CaCl_2$ molten salt based on SP1 and SP2 and compared with the experimental value [28]. It shows that the thermal conductivity calculated by SP1 is within the error of the experimental value, while the error of SP2 is much large. However, there are limited extant data on the thermal conductivity of molten chloride salts and the error of experimental measurements by different researchers is more than the test itself (uncertainty 10%). From the simulation results of thermal properties, both SP1 and SP2 potential parameters are more reasonable. Considering that the heat storage material used in the CSP system is eutectic molten salt, it is also necessary to analyze the thermal properties of molten calcium-containing multicomponent chlorides.

4.2. Verification of Binary Eutectic Salt NaCl-$CaCl_2$ Density

To further determine the applicability of $CaCl_2$ potential parameters, SP1 and SP2 were used to calculate the density of binary eutectic molten salt of 49.03 mol % NaCl-50.97 mol % $CaCl_2$. Because the potential parameter of NaCl [6] can well predict the high-temperature thermophysical properties and structural changes of chloride molten salt, the literature data of NaCl is directly selected. The simulated and experimental results are compared in Figure 3. Figure 3 shows that the simulated values of SP2 are basically consistent with the experimental values [4,29], and the error is within 0.5%, while the error of SP1 is within 8%. Probably because SP1 is the earliest simple potential energy model, the mixing rule is not suitable. Therefore, for the density calculation of binary NaCl-$CaCl_2$ eutectic molten salt, SP2 is more suitable as the BMH potential parameter of $CaCl_2$.

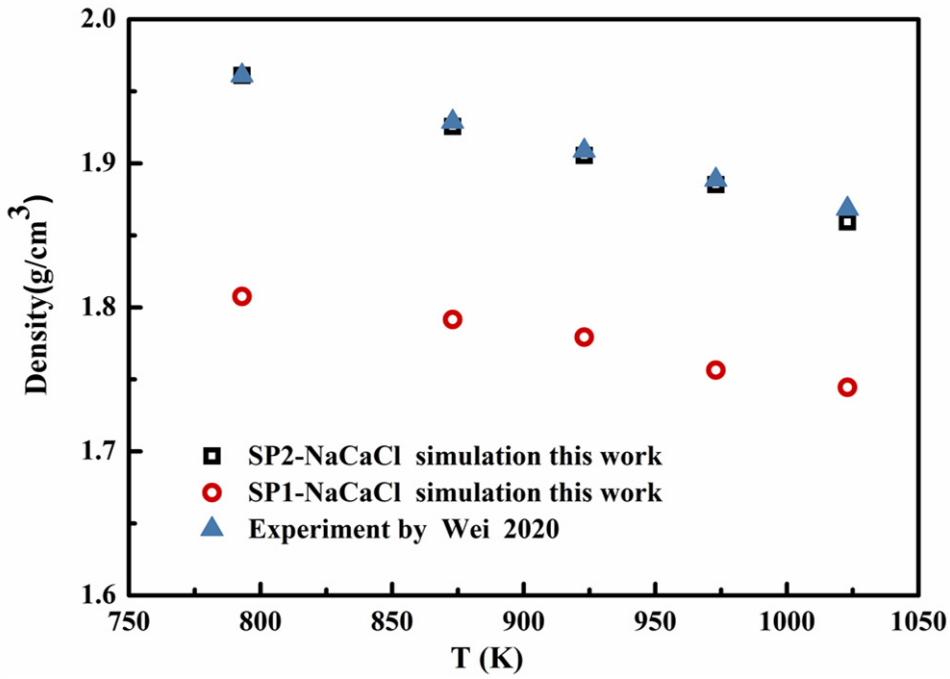

Figure 3. The density of binary eutectic salt NaCl-$CaCl_2$ vs. temperature [4].

4.3. Thermal Properties of Multi-Chlorine Eutectic Molten Salts

To further validate the applicability of parameter SP2. The thermophysical properties and microstructure of nine chloride eutectic molten salts in four systems, NaCl-$CaCl_2$ (49.03–50.97, 67.5–32.5, 22.5–77.5 mol %, named NaCa-1, NaCa-2 and NaCa-3 respectively), KCl-$CaCl_2$ (22.3–77.7, 31.9–68.1, 71.8–28.2 mol %, named KCa-1, KCa-2 and KCa-3 respectively), NaCl-$CaCl_2$-$MgCl_2$ (53.5–15–31.5, 45.1–26.3–28.6 mol %, named NaCaMg-1 and NaCaMg-2 respectively), and NaCl-$CaCl_2$-KCl (41.7–52.5–5.8 mol %, named NaCaK), were calculated as follows.

4.3.1. The Density of Chloride Molten Salts

Figure 4 shows the calculated densities of binary and ternary chloride molten salts with temperature. The density of NaCl-$CaCl_2$ (Figure 4a) and KCl-$CaCl_2$ (Figure 4b) binary molten salts calculated by SP2 is very compatible with the experimental result in the measurement temperature range [28], and the error is within 3%. The simulation results also provide accurate data of the higher temperature section that are difficult to measure. Figure 4c shows that the calculated density of calcium-containing ternary chloride molten salt is close to the experimental value, the error is less than within 4%, and the trend with temperature is also consistent. Therefore, the density of molten calcium-containing multicomponent chlorides can be predicted using the parameter SP2 at high temperatures.

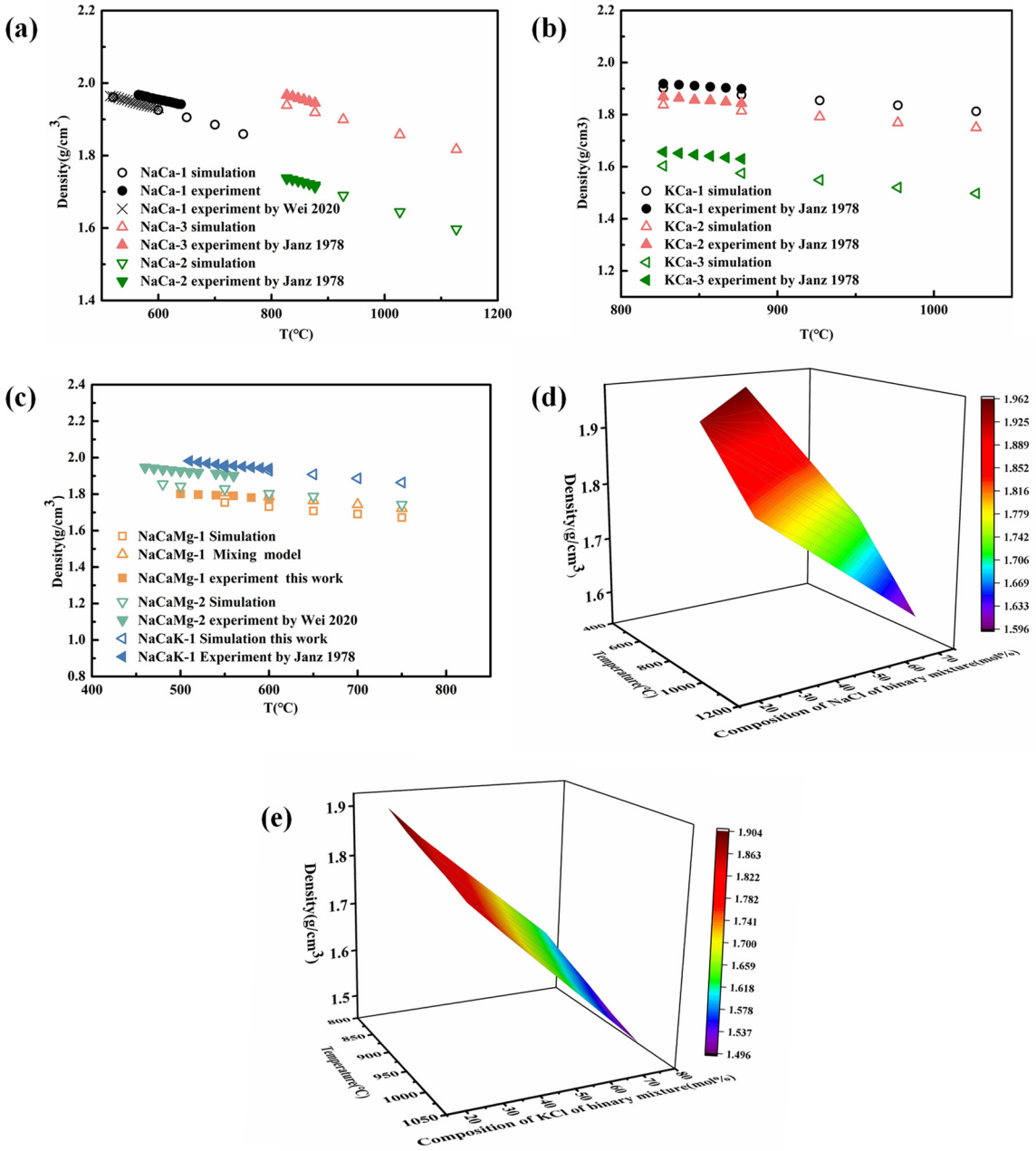

Figure 4. Density of chloride eutectic molten salts of (**a**) binary NaCl-$CaCl_2$, (**b**) binary KCl-$CaCl_2$, (**c**) ternary NaCl-$CaCl_2$-$MgCl_2$ vs. temperature, density of full composition of (**d**) NaCl-$CaCl_2$ and (**e**) KCl-$CaCl_2$ [4,28].

4.3.2. Specific Heat Capacity of Multicomponent Chloride Molten Salts

Specific heat capacity is a key indicator to characterize the heat storage capacity of molten salt materials. Figure 5 shows the calculation and measurement values of specific heat capacity of eutectic molten salt of multiple chlorides, and the comparison with the literature values. The specific heat capacity of molten NaCl-$CaCl_2$-1 in test temperature range is 1.006~1.105 J/(g·K), and the average specific heat capacity is 1.051 J/(g·K) (the data has been tabulated in the Supplementary Materials Tables S1 and S2). Figure 5a shows that the simulation result of specific heat capacity of molten NaCl-$CaCl_2$-1 is 1.06 J/(g·K), and the error between the simulation and experiment is only 0.8%. Differences between molten salt specific heat capacity values obtained by different researchers are greater than the experimental error. The error of specific heat capacity experimental values of NaCl-$CaCl_2$ (48–52 mol %) between the experimental data 1.10 J/(g·K) [5] and 1.00 J/(g·K) [30] is

10%. It can be seen that there is a certain error in the specific heat capacity measurement, probably due to the thermal contact of the thermocouple and also the error caused by the different types of instruments. Figure 5b,c show that the simulated value of ternary eutectic molten salt NaCl-$CaCl_2$-$MgCl_2$ (53.5–15–31.5 mol %) is 1.088 J/(g·K), and the error with the experimental average value 1.097 J/(g·K) [31] and 1.19 J/(g·K) [32] is 0.8% and 8.5%, respectively. For NaCl-$CaCl_2$-$MgCl_2$ (45.1–26.3–28.6 mol %), the error between the simulated value 1.11 J/(g·K) and the experimental value 1.04 J/(g·K) [4] is 6.7%. Moreover, the error between the simulated value 1.08 J/(g·K) of NaCl-$CaCl_2$-KCl and the experimental average value 1.00 J/(g·K) [30] and 0.91 J/(g·K) [4] was 8% and 18.6%, respectively. From the simulation results, SP2 can be used to predict the specific heat capacity data of molten salts of calcium-containing multicomponent chlorides without experimental conditions and experimental data, such as KCl-$CaCl_2$. Overall, the specific heat capacity of chloride molten salt is relatively low at about 1.0 J/(g·K), and the subsequent work will strengthen the specific heat capacity of chloride molten salt.

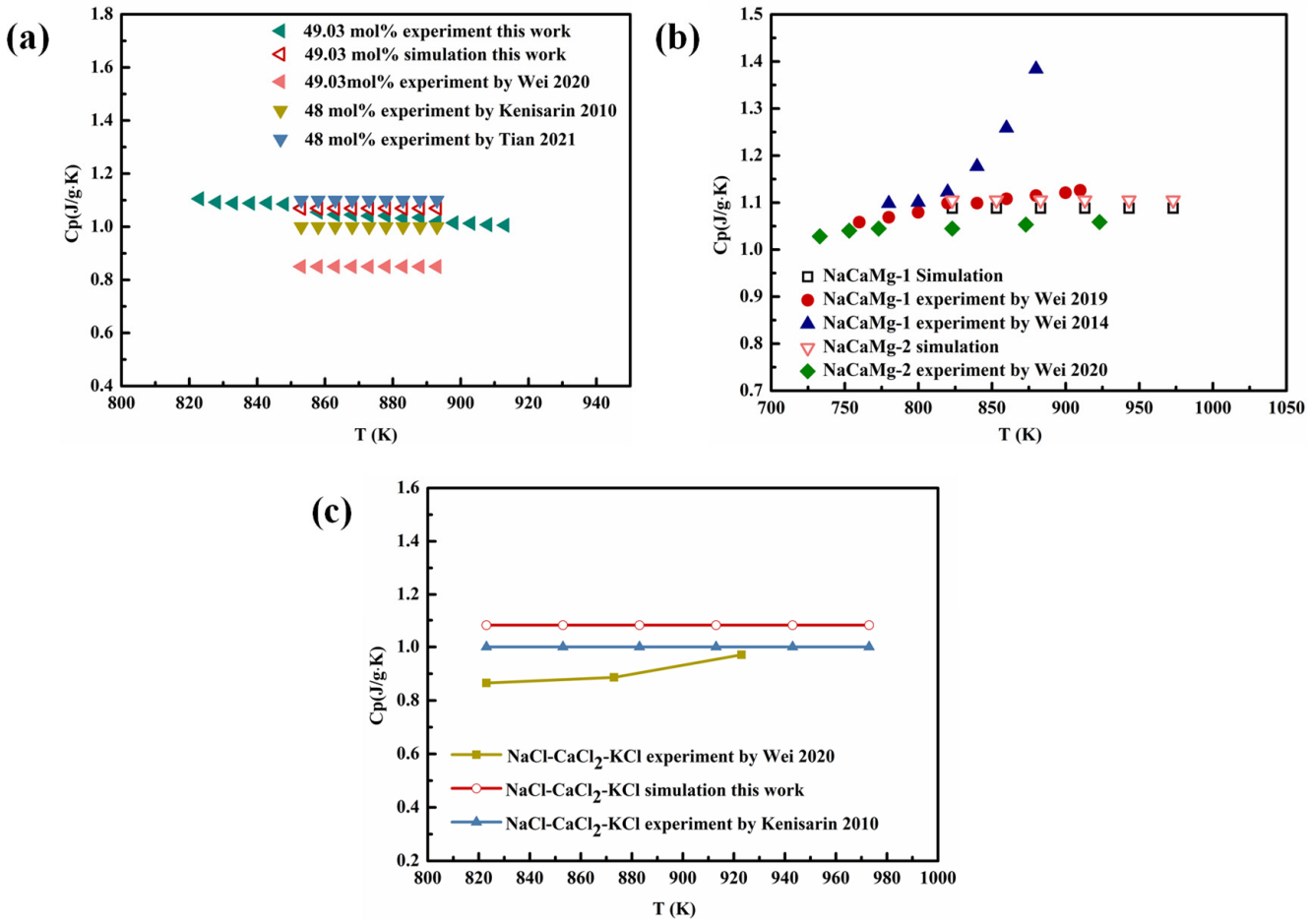

Figure 5. Specific heat capacities of chloride eutectic molten salts of (**a**) binary NaCl-$CaCl_2$, (**b**) ternary NaCl-$CaCl_2$-$MgCl_2$ and (**c**) NaCl-$CaCl_2$-KCl vs. temperature [4,5,30–32].

4.3.3. Thermal Conductivity of Multicomponent Chloride Molten Salts

Thermal conductivity is an important index to characterize the heat transfer performance of molten salt materials. By comparing the existing experimental data, it is verified that SP2 can be used to predict the thermal conductivity of multicomponent chlorides molten salt. Figure 6 is the thermal conductivity simulated results of binary and ternary molten salts based on SP2 simulation. The simulated proportion of NaCl-$CaCl_2$ (49.03–50.97 mol %) shown in Figure 6a is slightly different from that of the experiment [5], but all belong to the proportion of eutectic molten salt, and the deviation of

thermal conductivity simulation is ~16.9%. Figure 6b shows that the simulated results of NaCl-$CaCl_2$-$MgCl_2$ (53.5–15–31.5 mol %) are also larger than the experimental values [9], but the trend with temperature is consistent. It can be seen from the simulated results that there is a negative correlation between thermal conductivity and temperature, indicating that the simulated thermal conductivity is reasonable.

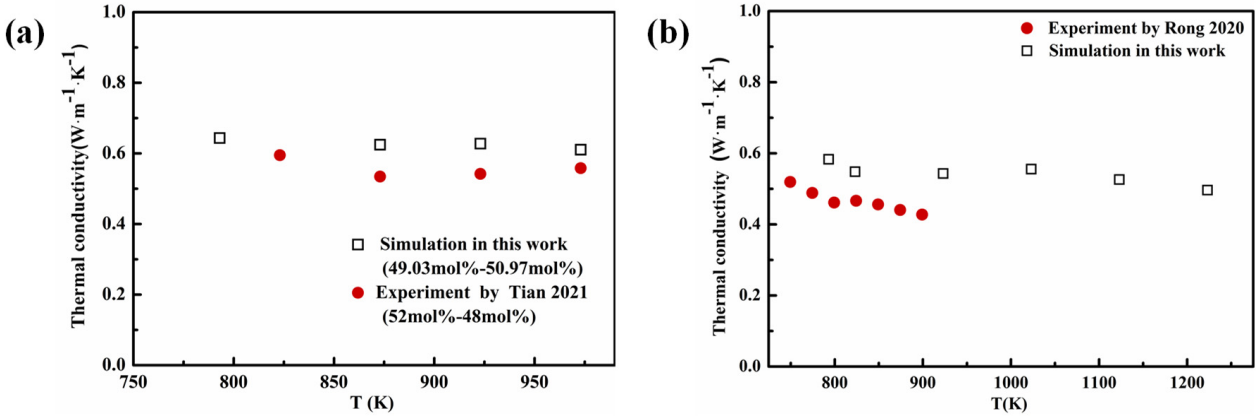

Figure 6. Thermal conductivity of chloride eutectic molten salts of (**a**) binary NaCl-$CaCl_2$ and (**b**) ternary NaCl-$CaCl_2$-$MgCl_2$ vs. temperature [5,9].

4.4. Structures of Multi-Chlorine Eutectic Molten Salt

In addition to predicting the heat transfer and heat storage performance of molten salt at high temperatures, the classical molecular dynamics simulation can also analyze the influence of temperature on the microstructure of molten salt. SP2 has been verified to be reasonable and widely applicable. The relationship between radial distribution, coordination number, and angle distribution of the above four systems and temperature can be analyzed below. Only the ratios of low eutectic points of four kinds of multi-component chloride molten salts were explored, which are NaCl-$CaCl_2$ (47.03–50.97 mol %), KCl-$CaCl_2$ (71.8–28.2 mol %), NaCl-$CaCl_2$-$MgCl_2$ (53.5–15–31.5 mol %), and NaCl-$CaCl_2$-KCl (41.7–52.5–5.8 mol %).

4.4.1. Radial Distribution Function and Coordination Number

Figure 7 shows the radial distribution and coordination number distribution of the four multi-chlorine eutectic molten salts. It can be seen from Figure 7 that the RDF of each ion pair in each molten salt has the first peak. With the increase of distance, the peak gradually decreases and then approaches to 1, indicating that the molten salt of multi-component chlorides has the characteristics of short-range order and long-range disorder. The first RDF peak of anion and cation pairs was sharper than that of cation pairs, such as the first peaks of Na^+-Cl^- and Ca^{2+}-Cl^- in NaCl-$CaCl_2$, indicating that the interaction between positive and negative ion pairs was stronger and the distance distribution between ions was more uniform. From the RDF of ternary molten salts shown in Figure 7c,d, it can be seen that the first peak of Mg^{2+}-Cl^- and Ca^{2+}-Cl^- is sharper than that of Na^+-Cl^- and K^+-Cl^-, and the coordination number curve has an obvious platform. The coordination number curve platform of Ca^{2+}-Cl^- is 6, and the coordination number of Mg^{2+}-Cl^- is 4, indicating that Ca^{2+} mainly exists in the multi-chloride molten salt with six coordination structures, and Mg^{2+} exists in four coordination structures. When the temperature increased from 823 K to 1023 K, the first peak height drop structure of anion and cation pairs of RDFs became loose. The first peak of positive ions shifts to the right, and the distance between cation associations increases with the increase of temperature, which reflects that the density should be reduced, which is consistent with the trend of density decrease with temperature shown in Figure 4.

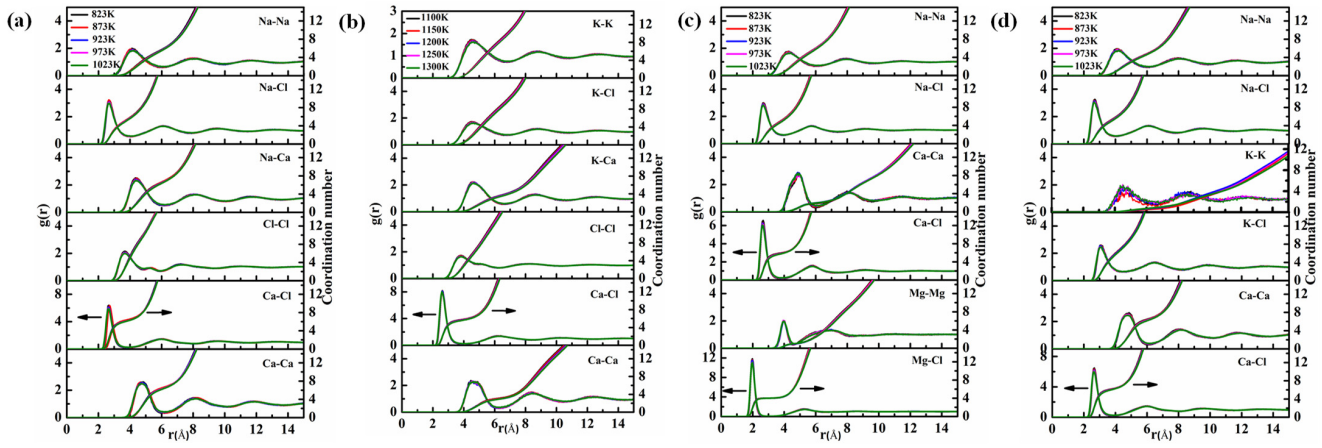

Figure 7. Radial distribution function (RDF) and coordination number curves of different chloride eutectic molten salts (**a**) NaCl-$CaCl_2$, (**b**) KCl-$CaCl_2$, (**c**) NaCl-$CaCl_2$-$MgCl_2$ and (**d**) NaCl-$CaCl_2$-KCl.

4.4.2. Bond Angle Distribution

As shown in Figure 8, in binary and ternary chloride molten salt systems, the bond angle distribution of Cl-Ca-Cl is mainly 90°, and a small part is 170°, forming a stable hexacoordinate octahedron structure, which is consistent with the coordination number in Figure 7. However, the Cl-Ca-Cl bond angle distribution in the NaCl-$CaCl_2$-$MgCl_2$ system is wider than that in other systems, because the Cl-Mg-Cl bond angle is mainly 109°, forming a stable tetrahedral structure and competing with Ca^{2+}. The bond angle distributions of Cl-Na-Cl and Cl-K-Cl in the four systems are mainly 90°, and the octahedral structure exists in eutectic molten salt.

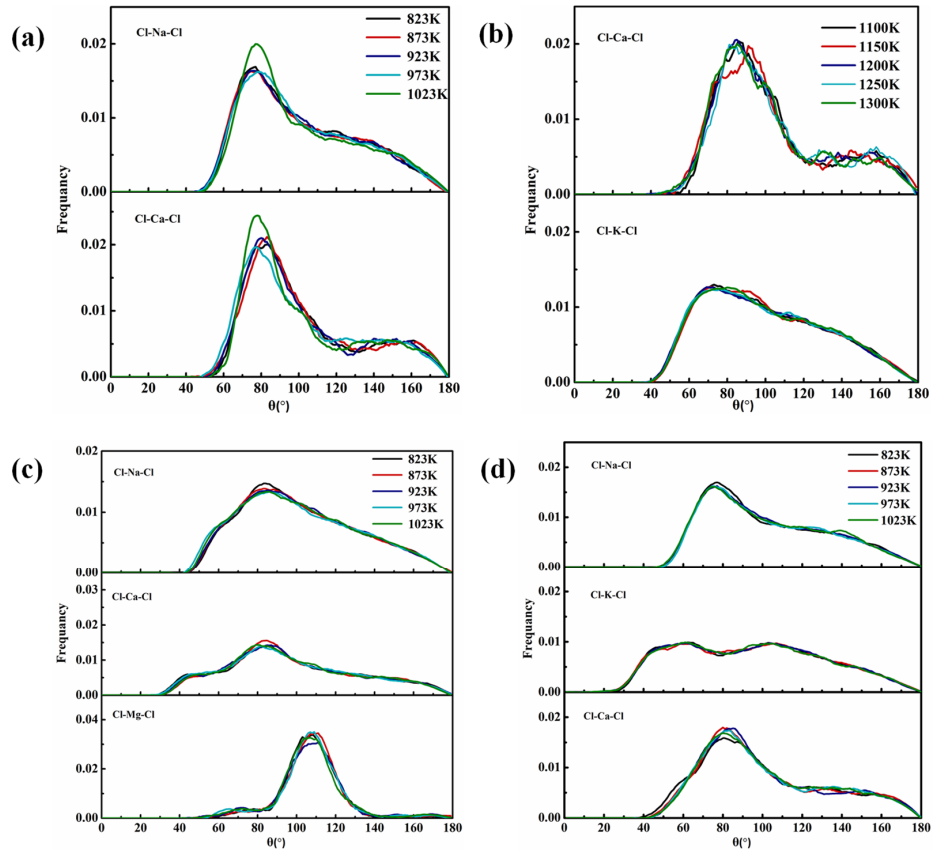

Figure 8. Bond angle distribution of different chloride eutectic molten salts (**a**) NaCl-$CaCl_2$, (**b**) KCl-$CaCl_2$, (**c**) NaCl-$CaCl_2$-$MgCl_2$ and (**d**) NaCl-$CaCl_2$-KCl.

5. Conclusions

Due to the lack of potential function of alkali earth metal chlorides, molecular dynamics simulation of molten chloride salts is mainly applied to alkali metal chlorides, but there are few simulation studies on eutectic calcium-containing molten chlorides. In this paper, SP2 was determined as the BMH potential parameter of $CaCl_2$ by comparing the classical molecular dynamics simulation results with the experimental values. The structure of unit $CaCl_2$ is consistent with the experimental value. The error of density between the simulated and the experimental value is within 3%, while the error of the simulated thermal conductivity is relatively large.

The applicability of SP2 in molten salts of multiple chlorides with different ratios was verified. The simulated values of density and specific heat capacity of four multi-component chloride molten salts are in good agreement with the experimental values, and the simulated values of thermal conductivity are also large. However, there is a certain error in the measurement of the thermal conductivity of the molten chloride salt with high working temperature. From the negative correlation between the simulated thermal conductivity and temperature, the thermal conductivity of the molten chloride salt containing calcium calculated by SP2 is reasonable. The simulation results of the structure show that $CaCl_2$ mainly exists in a hexacoordinate octahedral structure in multi-component chloride molten salts.

Supplementary Materials: The following supporting information can be downloaded at: https://www.mdpi.com/article/10.3390/en15238878/s1, Table S1: The experiment result of the specifie heat capacity of molten NaCl-$CaCl_2$ (49.03–50.97 mol %) in test temperature range; Table S2: The experiment result of density of molten NaCl-$CaCl_2$ (49.03–50.97 mol %) and NaCl-$CaCl_2$-$MgCl_2$ (53.5–15–31.5 mol %) in test temperature range.

Author Contributions: Conceptualization, X.W. and W.W.; methodology, D.C. and S.L.; software, S.L.; validation, X.W., D.C. and W.W.; formal analysis, D.C. and S.L.; investigation, W.W.; resources, J.D. and J.L.; data curation, X.W. and D.C.; writing—original draft preparation, X.W. and D.C.; writing—review and editing, W.W. and S.L.; visualization, D.C. and S.L.; supervision, X.W.; project administration, J.D. and X.W.; funding acquisition, X.W. and J.D. All authors have read and agreed to the published version of the manuscript.

Funding: This work was supported by the key projects of National Natural Science Foundation of China (52036011).

Data Availability Statement: Data available on request.

Acknowledgments: We thank the computer time from Tianhe-2 system at National Supercomputer Center in Guangzhou.

Conflicts of Interest: The authors declare no conflict of interest.

References

1. Roper, R.; Harkema, M.; Sabharwall, P.; Riddle, C.; Chisholm, B.; Day, B.; Marotta, P. Molten salt for advanced energy applications: A review. *Ann. Nucl. Energy* **2022**, *169*, 108924. [CrossRef]
2. Rice, S.A.; Klemperer, W. Spectra of the Alkali Halides. II. The Infrared Spectra of the Sodium and Potassium Halides, RbCl, and CsCl. *J. Chem. Phys.* **1957**, *27*, 573–579. [CrossRef]
3. Dunn, R.I.; Hearps, P.J.; Wright, M.N. Molten-Salt Power Towers: Newly Commercial Concentrating Solar Storage. *Proc. IEEE* **2012**, *100*, 504–515. [CrossRef]
4. Wei, X.; Xie, P.; Zhang, X.; Wang, W.; Lu, J.; Ding, J. on preparation and thermodynamic properties of chloride molten salt materials. *CIESC J.* **2020**, *71*, 2423–2431. [CrossRef]
5. Tian, H.; Wang, W.; Ding, J.; Wei, X. Thermal performance and economic evaluation of NaCl–$CaCl_2$ eutectic salt for high-temperature thermal energy storage. *Energy* **2021**, *227*, 120412. [CrossRef]
6. Pan, G.-C.; Ding, J.; Wang, W.; Lu, J.; Li, J.; Wei, X. Molecular simulations of the thermal and transport properties of alkali chloride salts for high-temperature thermal energy storage. *Int. J. Heat Mass Transf.* **2016**, *103*, 417–427. [CrossRef]
7. Xie, W.; Ding, J.; Pan, G.; Fu, Q.; Wei, X.; Lu, J.; Wang, W. Heat and mass transportation properties of binary chloride salt as a high-temperature heat storage and transfer media. *Sol. Energy Mater. Sol. Cells* **2020**, *209*, 110415. [CrossRef]

8. Bu, M.; Liang, W.; Lu, G.; Yu, J. Static and dynamic ionic structure of molten $CaCl_2$ via first-principles molecular dynamics simulations. *Ionics* **2020**, *27*, 771–779. [CrossRef]
9. Rong, Z.; Ding, J.; Wang, W.; Pan, G.; Liu, S. Ab-initio molecular dynamics calculation on microstructures and thermophysical properties of NaCl–$CaCl_2$–$MgCl_2$ for concentrating solar power. *Sol. Energy Mater. Sol. Cells* **2020**, *216*, 110696. [CrossRef]
10. Rong, Z.; Pan, G.; Lu, J.; Liu, S.; Ding, J.; Wang, W.; Lee, D.-J. Ab-initio molecular dynamics study on thermal property of NaCl–$CaCl_2$ molten salt for high-temperature heat transfer and storage. *Renew. Energy* **2021**, *163*, 579–588. [CrossRef]
11. Igarashi, K.; Tajiri, K.; Asahina, T.; Kosaka, M. Structural Study of Molten $CaCl_2$-KCl System. *Mater. Sci. Forum* **1991**, *73–75*, 79–84. [CrossRef]
12. Igarashi, K.; Okamoto, Y.; Mochinaga, J. X-ray Diffraction Study of Molten $CaCl_2$-KCl System. *ECS Proc. Vol.* **1987**, *7*, 175–184. [CrossRef]
13. Martínez, L.; Andrade, R.; Birgin, E.G.; Martínez, J.M. PACKMOL: A package for building initial configurations for molecular dynamics simulations. *J. Comput. Chem.* **2009**, *30*, 2157–2164. [CrossRef] [PubMed]
14. Zhu, S.; Jiang, W.; Xu, Y.; Guo, J. Interionic potentials and their parameters in the alkali halides. *J. Guangxi Univ.* **2004**, *3*, 202–206. [CrossRef]
15. Baughan, E.C. The repulsion energies in ionic compounds. *Trans. Faraday Soc.* **1959**, *55*, 736–752. [CrossRef]
16. Woodcock, L.V.; Angell, C.A.; Cheeseman, P. Molecular dynamics studies of the vitreous state: Simple ionic systems and silica. *J. Chem. Phys.* **1976**, *65*, 1565–1577. [CrossRef]
17. Yuen, P.S.; Murfitt, R.M.; Collin, R.L. Interionic forces and ionic polarization in alkaline earth halide crystals. *J. Chem. Phys.* **1974**, *61*, 2383–2393. [CrossRef]
18. Tosi, M.; Fumi, F. Ionic sizes and born repulsive parameters in the NaCl-type alkali halides—II: The generalized Huggins-Mayer form. *J. Phys. Chem. Solids* **1964**, *25*, 45–52. [CrossRef]
19. Lu, J.; Yang, S.; Rong, Z.; Pan, G.; Ding, J.; Liu, S.; Wei, X.; Wang, W. Thermal properties of KCl–$MgCl_2$ eutectic salt for high-temperature heat transfer and thermal storage system. *Sol. Energy Mater. Sol. Cells* **2021**, *228*, 111130. [CrossRef]
20. Smith, F.T. Atomic Distortion and the Combining Rule for Repulsive Potentials. *Phys. Rev. A* **1972**, *5*, 1708–1713. [CrossRef]
21. Ping, H.S.; Yoshida, F. Ionic Properties of the Metal-Salt Solution $Ca_x(CaCl_2)_{1-x}$. *J. Phys. Soc. Jpn.* **1997**, *66*, 392–395. [CrossRef]
22. Plimpton, S. Fast Parallel Algorithms for Short-Range Molecular Dynamics. *J. Comput. Phys.* **1995**, *117*, 1–19. [CrossRef]
23. Scott, R.; Allen, M.P.; Tildesley, D.J. Computer Simulation of Liquids. *Math. Comput.* **1991**, *57*, 442–444. [CrossRef]
24. Müller-Plathe, F. A simple nonequilibrium molecular dynamics method for calculating the thermal conductivity. *J. Chem. Phys.* **1997**, *106*, 6082–6085. [CrossRef]
25. Jayaraman, S.; Thompson, A.P.; von Lilienfeld, O.A.; Maginn, E. Molecular Simulation of the Thermal and Transport Properties of Three Alkali Nitrate Salts. *Ind. Eng. Chem. Res.* **2010**, *49*, 559–571. [CrossRef]
26. Biggin, S.; Enderby, J.E. The structure of molten calcium chloride. *J. Phys. C Solid State Phys.* **1981**, *14*, 3577–3583. [CrossRef]
27. David, R. *Handbook Chemistry and Physics*, 84th ed.; CRC Press: Boca Raton, FL, USA, 2003.
28. Janz, G.J.; Allen, C.B.; Bansal, N.P.; Murphy, R.M.; Tomkins, R.P.T. Physical properties data compilations relevant to energy storage. II. Molten Salts: Data on Single and Multi-Component Salt Systems. In *Physical Properties Data Compilations Relevant to Energy Storage*; National Bureau of Standards: Gaithersburg, MD, USA, 1978.
29. Grjotheim, K.; Holm, J.L.; Lillebuen, B.; Øye, H.A. Densities and excess molar volumes of binary and ternary melts of $MgCl_2$, $CaCl_2$ and AlkCl. *Trans. Faraday Soc.* **1971**, *67*, 640–648. [CrossRef]
30. Kenisarin, M.M. High-temperature phase change materials for thermal energy storage. *Renew. Sustain. Energy Rev.* **2010**, *14*, 955–970. [CrossRef]
31. Wei, X.; Zhang, X.; Ding, J.; Wang, W.; Lu, J. The effect of nano-MgO on thermal properties of ternary chloride fluid. *Innov. Solut. Energy Transit.* **2019**, *158*, 773–778. [CrossRef]
32. Wei, X.; Song, M.; Peng, Q.; Ding, J.; Yang, J. A new ternary chloride eutectic mixture and its thermo-physical properties for solar thermal energy storage. *Energy Procedia* **2014**, *61*, 1314–1317. [CrossRef]